Robust Beat-to-Beat Interval from Wearable PPG using RLS and SSA

Tanuka Bhattacharjee, Anirban Dutta Choudhury and Arpan Pal

***Abstract*— Ambulatory Photoplethysmogram (PPG) is a more user-friendly choice for continuous cardiac monitoring as compared to Electrocardiogram (ECG). However, wearable PPG is often prone to motion artefacts. In this paper, we propose a novel pipeline for motion-resistant beat-to-beat interval extraction from noisy PPG. Firstly, the effects of motion artefacts are minimized by using Adaptive Recursive-Least-Square (RLS) Filtering and Singular Spectrum Analysis (SSA). Next, the signal peaks are identified and their locations are corrected by weighted local interpolation. Finally, outlier peak-to-peak intervals are marked as incorrigible. Experimental validation on the training dataset of IEEE Signal Processing Cup 2015 reveals that the proposed method achieves 1.68% *mean peak detection error rate* and 11.32 milliseconds *mean absolute error* of detected beat-to-beat intervals. The metric values outperform those obtained by the state-of-the-art techniques by at least 12.58 and 5.74 times respectively.**

I. Introduction

Since the advent of medical sciences spanning last century, Non-Communicable Diseases (NCDs) have emerged as the biggest threat to human life, killing 41 million people each year, accounting to 71% of all deaths globally. Moreover, 85% of those premature deaths (between 30 and 69 years) take place in developing countries [1]. Cardio-Vascular Diseases (CVDs) are the *numero uno* killer amongst NCDs, followed by cancers, respiratory diseases and diabetes. In south-east Asian countries like India, the numbers are even worse when compared to global burden of CVD death [2].

There have been numerous works on non-invasive detection of Chronic Ischemic Heart Diseases (IHD; ICD-10 Diagnosis Code I25) e.g. Coronary Artery Disease (CAD; ICD-10 Diagnosis Code I25.9) [3]. Researchers have worked on various signals e.g., Phonocardiogram (PCG), Electrocardiogram (ECG) and Photoplethysmogram (PPG) to detect CAD [4], [5]. However, cardiac rhythm problems e.g., Atrial Fibrillation (AF), Flutter and other Arrhythmias (ICD-10 Diagnosis Code I48 and I49 respectively) are relatively lesser explored. In order to detect cardiac rhythm problems such as AF, the most important requirement is precise calculation of beat-to-beat cardiac cycles. Very recently, Physionet Challenge 2017 opened up a global competition for the development of algorithms to detect if a single short ECG lead recording ($<$ 1 minute length) reveals normal sinus rhythm, AF, an alternative rhythm, or is too noisy to be classified [6]. One of the winners [7] claimed $\approx$ 83% F1-score on unseen test data provided by the competition organizers.

Though single-channel ECG is more user-friendly as compared to 12 channel ECG, one still needs to set a personal alarm to touch the electrodes in a smart watch/ smart phone accessory in order to capture his/her ECG. Hence, a continuous ECG may prove to be a overkill for the hand-held device. On the other hand, the consumer market is flooded with devices capable of recording PPG 24x7 [8]. These off-the-shelf wearables are often used to calculate average heart rate [9]. Given the requirement of the 24x7 non-invasive detection of irregular cardiac rhythms and the proliferation of low-cost wearables, we see an excellent opportunity of estimation of beat-to-beat intervals from PPG signal.

The authors are with Embedded Systems and Robotics, TCS Research and Innovation, India, {bhattacharjee.tanuka, anirban.duttachoudhury, arpan.pal}@tcs.com

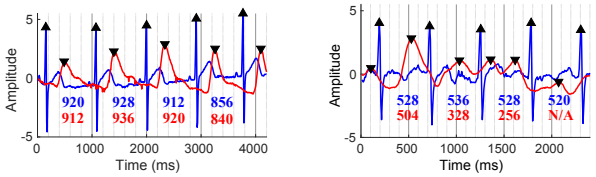

(a) Clean PPG (b) PPG with motion artefact

Fig. 1. Waveforms and estimated beat-to-beat intervals of simultaneous PPG (—) and ECG (—); here ▲: ECG R-peak, ▼: PPG peak; PPG intervals are chosen for comparison as elaborated in Section IV-A

The PPG signal is essentially the volumetric measure of human body fluid which in our case translates to blood volume through wrist. Physiologically the systolic peaks of the PPG signal should follow the ECG signal R-peaks. The primary concern in PPG-based beat-to-beat interval estimation is that the signal is highly prone to motion artefacts. Regular day-to-day activities can heavily distort the signal, thereby making systolic peak detection very challenging. Fig. 1(a) shows a clean PPG captured during rest where the systolic peaks can be easily identified and the beat-to-beat intervals closely follow those of ECG. The protocol for comparing the beat-to-beat intervals obtained from ECG and PPG is given in Section IV-A. Fig. 1(b) shows a PPG segment affected by motion artefacts. Detection of peaks from this distorted waveform gives rise to fluctuating measures of beat-to-beat intervals, thereby making the signal appear as one revealing the symptoms of irregular rhythm. In this context, we have the following aims in this paper:

1) Identify PPG segments which are incorrigible.
2) Clean the rest of the PPG signal and detect the systolic peak to systolic peak (SPSP) intervals.
3) Validate our results against gold standard of beat-to-beat intervals (extracted from ECG signal).

Several PPG motion artefact removal works are present in the literature which exploit acceleration signals. Zhang *et al.* [9] proposed the TROIKA framework, where a noisy PPG signal was decomposed by Singular Spectrum Analysis (SSA). The clean PPG was reconstructed after rejecting

978-1-5386-1311-5/19/$31.00 ©2019 IEEE

the motion artefact components by frequency domain comparison between PPG components obtained by SSA and simultaneous acceleration signals. Later, Zhang proposed an improved framework JOSS [10], which jointly estimated the sparse spectra of noisy PPG and acceleration signals. Spectrum subtraction was then performed to eliminate the motion components from PPG spectrum. In [11] and [12] the authors combined adaptive Recursive-Least-Square (RLS) filtering with SSA to develop a hybrid PPG motion artefact removal algorithm. Cascaded Normalized Least Mean Square adaptive filtering was used by Xie *et al.* [13]. Xiong *et al.* [14], on the other hand, modeled motion artefact removal as a Multi-Channel Spectral Matrix Decomposition optimization problem. Though all of the above-cited literature dealt with PPG motion artefact removal, they did not attempt to identify beat-to-beat/ SPSP intervals. Rather their aim was to obtain average heart rate in a time window, for which they mostly adapted frequency domain approaches.

Sun *et al.* [15] performed multi-scale PPG signal analysis using Empirical Mode Decomposition and Hilbert Transform for motion artefact reduction. The systolic peaks were then located by finding the positive-to-negative sign changes of the derivative of the cleaned PPG. Han and Kim [16] employed adaptive Least Mean Square (LMS) filtering for PPG motion artefact cancellation and a downward zero-crossing based peak detection algorithm for systolic peak identification. Jang *et al.* [17] filtered the noisy PPG by cascaded recursive digital filters and utilized the Slope Sum Function for peak detection. Moreover, they handled the wrongly identified and missed peaks by rule-based post-processing. Vadrevu *et al.* [18] decomposed the motion-contaminated PPG by Stationary Wavelet Transform and computed Multi-scale Sums and Products (MSP) of selected PPG sub-bands to enhance the systolic peaks and suppress the noise. Peak detection on Shannon entropy envelope of MSP was then performed by Gaussian derivative filtering and positive zero-crossing detection. In spite of having those attempts, still there exists wide room for improvement in beat-to-beat/ SPSP interval detection from noisy PPG. Here comes the contributions of this paper, as summarized below.

1) A novel pipeline of signal preprocessing, motion artefact removal, peak detection and post-processing is proposed for SPSP interval extraction from noisy PPG.
2) Different post-processing techniques for peak correction are explored.
3) An outlier detection approach is used for identifying the erroneous SPSP interval detections and the corresponding PPG segments are marked as incorrigible.

II. Dataset

This paper uses the publicly available training dataset of the IEEE Signal Processing Cup 2015 [9]. This dataset contains synchronous two-channel wrist-PPG (NP_1, NP_2), three-axis accelerometer (A_x, A_y, A_z) and single-channel chest-ECG (E_g) data of 12 subjects recorded at 125 Hz sampling frequency. During data capture, subjects ran on a treadmill while the speed was varied as follows: rest (30 sec) $\rightarrow$ 6-8 km/hr (1 min) $\rightarrow$ 12-15 km/hr (1 min) $\rightarrow$ 6-8 km/hr (1 min) $\rightarrow$ 12-15 km/hr (1 min) $\rightarrow$ rest (30 sec). The subjects moved the hand with the wrist-band purposely, even during rest, to introduce brief motion artefacts. An illustrative set of synchronous waveforms during 6-8 km/hr run is shown in Fig. 2. The high activities in the acceleration channels confirm that the primary noise present in the captured PPG arises from motion. The ECG being captured by wet sensor that sticks firmly to the subject's chest, this signal is much less susceptible to motion artefacts than PPG. Hence ECG can be treated as the gold standard in this paper.

III. Methodology

This section describes several baseline methods used to design a novel pipeline for beat-to-beat interval estimation using the noisy PPG shown in Fig. 2.

A. Baseline 1 : Preprocessing & Peak Detection

This very first approach towards our objective comprises only the basic steps of preprocessing and peak detection.

1) Preprocessing: We follow a three stage process, as follows.

i. Segmentation: Firstly, the captured PPG signals are divided into consecutive segments of 30 sec in order to make this method suitable for real-time application.

ii. Filtering: The resting heart rate of a healthy adult can vary in 40-100 bpm ($\approx 0.6 - 1.6$ Hz) [19]. The heart rate can rise up to around 200 bpm (≈ 3.3 Hz) [20] during extensive physical activities. Hence, as a second preprocessing step, the PPG segments are filtered in 0.6-3.3 Hz by a 10^{th} order Infinite Impulse Response (IIR) Butterworth Band-Pass Filter (BPF) to remove components outside this frequency band of interest. The filter is applied forward and backward to avoid any introduction of phase shift.

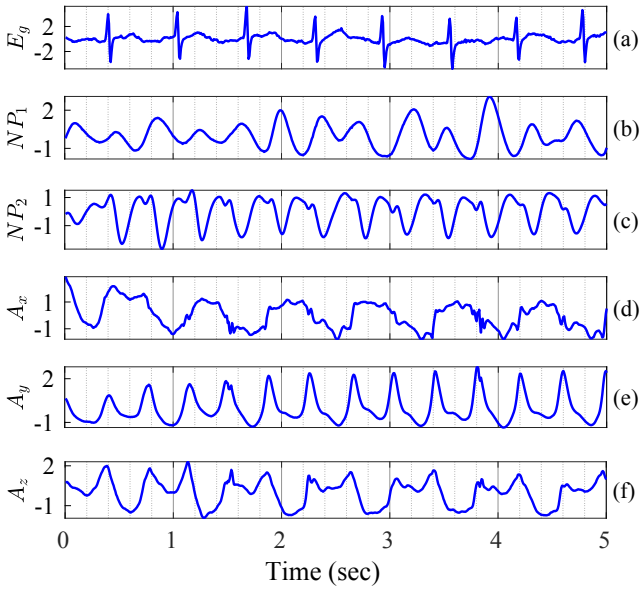

Fig. 2. Illustrative examples of (a) gold standard ECG (E_g), (b) noisy PPG channel 1 (NP_1), (c) noisy PPG channel 2 (NP_2), (d) x-axis acceleration (A_x), (e) y-axis acceleration (A_y), and (f) z-axis acceleration (A_z)

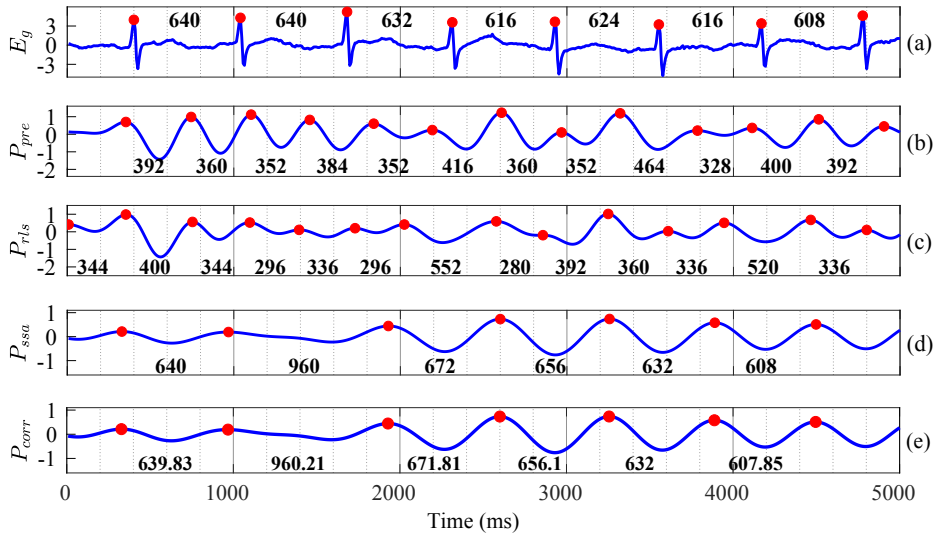

Fig. 3. Effects of different steps of the proposed algorithm on the illustrative example of Fig. 2: (a) gold standard ECG (E_g), (b) Baseline 1 (P_{pre}), (c) Baseline 2 - RLS (P_{rls}), (d) Baseline 2 - RLS + SSA (P_{ssa}), and (e) Baseline 3 - weighted local interpolation (P_{corr}); here the detected peaks are marked by red dots and the corresponding peak-to-peak intervals are reported in ms

iii. Normalization: Finally, the filtered PPG signals are normalized to zero mean and unit variance by Z-score normalization to bring all signals to the same scale of comparison. Since multiple PPG channels are available, their mean is considered for the subsequent steps.

2) Peak detection: The samples of the preprocessed PPG signal having amplitude larger than those of the neighboring samples on either side are identified as the systolic peaks of the signal. The differences between the locations of consecutive peaks are obtained to determine the SPSP intervals.

The preprocessed form P_{pre} of the noisy PPG of Fig. 2 is shown in Fig. 3(b). It can be observed that several spurious peaks are identified in the PPG waveform. Moreover, comparison with the RR intervals obtained from E_g (Fig. 3(a)) suggests that estimates of SPSP intervals are far from accurate. Therefore only conventional preprocessing is not sufficient for removing the artefacts of concern.

B. Baseline 2: Motion Artefact Removal using RLS and SSA

The proposed approach uses the three-axis acceleration signals to model the noise due to motion. These acceleration signals are also preprocessed as per the steps described in Section III-A.1. The proposed motion artefact removal process is following.

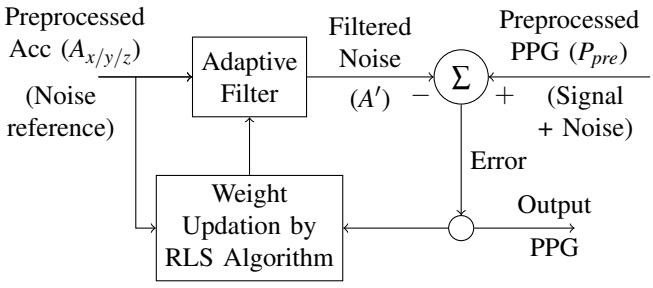

Fig. 4. Block Diagram of an Adaptive RLS Filter Module

1) Adaptive Recursive-Least-Square (RLS) Filtering: Motion artefacts are known to be additive to the PPG signal. Adaptive filtering algorithms, e.g. LMS, RLS, perform well in such additive noise cancellation applications. Here, an adaptive Finite Impulse Response (FIR) filter employing conventional RLS technique is used as the first step of removing motion interferences from the PPG signal. RLS is chosen over LMS due to its higher convergence speed [21] and FIR filter is used because of the inherent stability. Firstly, RLS filtering is performed on the preprocessed PPG signal to suppress the artefacts resulting from motion along x-axis by using the x-axis acceleration as the reference signal. Subsequently, the output residual PPG signal is processed twice more by this adaptive RLS filtering using the y-axis and z-axis accelerations sequentially as the references. The block diagram of one RLS filter module is shown in Fig. 4. In this paper, the filter order and forgetting factor are empirically chosen as 3 and 0.999 respectively.

Fig. 3(c) shows the waveform P_{rls} obtained after subjecting the preprocessed PPG P_{pre} of Fig. 3(b) to adaptive RLS filtering. It is to be noted that, though the SPSP interval estimates are still inaccurate, a significant fraction of the spurious peaks are attenuated by a remarkable margin.

2) Singular Spectrum Analysis (SSA): In order to have profound motion artefact removal performance, the PPG signal P_{rls} obtained after adaptive RLS filtering is decomposed into a set of *Reconstructed Components* (RCs) by SSA [22]. Here a window length of 2 sec is used for constructing the trajectory matrix. SSA decomposes a signal into trend, oscillation and noise components. The oscillatory components appear in pairs, both of which represent the same frequency. Corresponding to *each pair of oscillatory components*, there exists a *pair of eigen-values* of the covariance of trajectory matrix, which have nearly equal magnitudes. Higher the relative magnitude of the eigen-value pair, more significant is the corresponding oscillation in the signal.

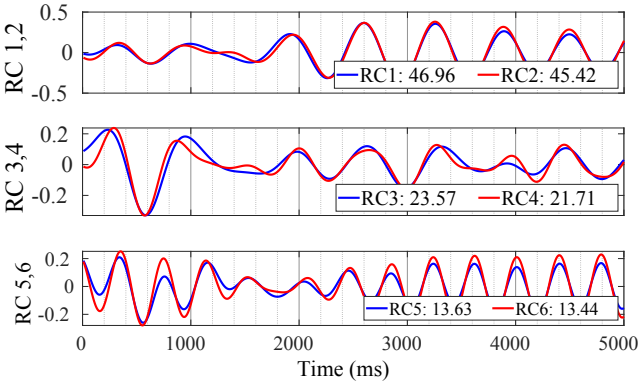

Fig. 5. Reconstructed Components (RCs) corresponding to the six highest eigen-values (given in the legend) of PPG P_{rls} obtained by SSA

Fig. 5 illustrates the RCs corresponding to the six highest eigen-values of P_{rls}. The highest eigen-value pair is ≈ 2 times the next. Therefore RC1-2 are much more significant than the rest. Hence, in the proposed method the RCs corresponding to the *two highest eigen-values* are considered. Since the pre-processed PPG signal undergoes adaptive noise cancellation before SSA decomposition, the dominant motion artefacts are already minimized to a remarkable extent, as can be seen in Fig. 3(c). Thus the most significant component remaining in the PPG signal should be the cardiac rhythm itself, which we aim to capture. So the most significant oscillatory component-pair obtained from SSA are used to reconstruct the clean PPG. This clean PPG is found to be of sinusoidal nature where the dicrotic peaks are mostly eliminated, thus simplifying the systolic peak detection procedure.

The clean PPG signal P_{ssa} obtained after SSA processing, along with the detected peaks are shown in Fig. 3(d). Visibly the SPSP intervals obtained at this stage relate closely to the ground truth RR intervals of Fig. 3(a).

C. Baseline 3: Peak Correction

The precision of the systolic peak locations detected by Baseline 2 is limited by the sampling frequency (f_s) of the captured signal, which is 125 Hz in our case. According to the Nyquist Theorem, f_s should be at least twice the maximum frequency present in the signal in order to faithfully capture all the details. Hence, f_s (= 125 Hz) results into a faithful error resolution of $2 \times 1/f_s$ (= 16 ms), which can be significantly high for low f_s. This paper overcomes this issue by applying one of the following methods.

i. Weighted Local Interpolation: In this method, the location l_i of the i^{th} systolic peak of the cleaned PPG P_{ssa} is refined by considering its 5 nearest neighboring data-points on either side, as given below.

$$\tilde{l_i} = \frac{\sum_{k=-5}^{5} P_{ssa}(l_i+k) * (l_i+k)}{\sum_{k=-5}^{5} P_{ssa}(l_i+k)} \quad (1)$$

ii. Polynomial Fitting: Here also the same segment of P_{ssa} is extracted which contains the concerned systolic peak location l_i and its 5 nearest neighboring data-points on either side. The coefficients of the best fit 3^{rd} order polynomial for this extracted segment are computed. The real roots of the derivative of this polynomial are determined and the one corresponding to maximum amplitude of P_{ssa} is chosen as the refined systolic peak.

iii. Global Interpolation: Prior to performing peak detection, the clean PPG time-series P_{ssa} is interpolated to 1000 Hz by cubic spline interpolation. Increasing the sampling frequency beyond 1000 Hz seems unnecessary as the performance enhancement is not significant.

It is found that all three of the described methods achieve very similar performances. However, the computational burden of weighted local interpolation is the least. It requires $\approx 3.95 \times 10^9$ instructions to process a 30 sec data segment whereas polynomial fitting and global interpolation take $\approx 4.72 \times 10^9$ and $\approx 4.39 \times 10^9$ instructions respectively. The refined SPSP intervals obtained from the PPG signal of Fig. 3(d) by weighted local interpolation are shown in Fig. 3(e).

D. Final method: Outlier Removal

As the final step, we propose to recognize the incorrigible SPSP intervals. The motivation behind this is to get rid of the cycles which are beyond correction and if not removed, tend to introduce considerable error in beat-to-beat interval estimation. For this purpose, the computed SPSP intervals are subjected to the process of outlier removal over 6 sec windows with 2 sec overlap. Let the median SPSP interval of any window be m_{sp}. The intervals lying below $m_{sp} - 0.4 * m_{sp}$ are considered to be probable errors and are merged with that adjacent interval which has lower duration among the two. On the other hand, intervals lying above $m_{sp} + 0.4 * m_{sp}$ along with the immediately preceding peaks are discarded. The corresponding portions of the PPG signal are marked as incorrigible by the proposed algorithm. It is suggested in [23] that beat-to-beat intervals can vary by $\approx 18\%$ for healthy individuals. We are imposing a much more relaxed constraint of 40% in order to allow the cycles arising from arrythmia while discarding only motion-affected cycles which are beyond repair. The complete flow of the proposed final method is summarized in Fig. 6.

The black PPG segment in Fig. 7 is marked as incorrigible. It can be seen that the corresponding SPSP interval is found as 960.21 ms. This is significantly different from the rest intervals (607.85 - 671.81 ms), which is unlikely for a healthy subject. Hence the proposed algorithm can correctly identify the PPG regions which could not be reconstructed.

IV. Results

A. Validation Protocol

We use ECG R-peaks identified by the modified Pan Tompkin's algorithm [24] as the ground truth for experimental validation. The improper R-peak identifications are manually corrected wherever possible. The characteristic points of PPG lag those of ECG. Hence, each PPG systolic peak should be positioned somewhere in between two consecutive R-peaks. Based on this fact, the following rules are developed for performance evaluation of the proposed method.

1) If no PPG peak is identified between a pair of R-peaks, then a False Negative (FN) occurs.

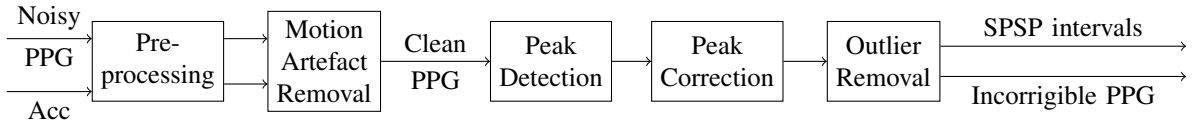

Fig. 6. Flow-diagram of Final Method

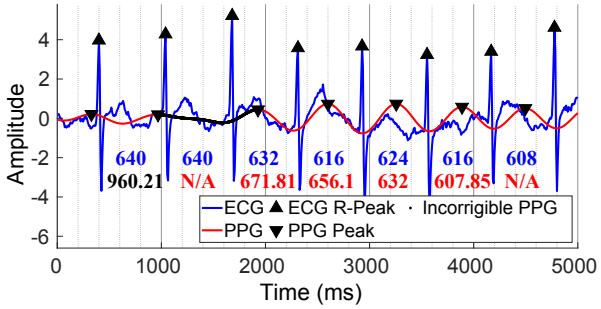

Fig. 7. Effect of Outlier Removal on the PPG signal of Fig. 3(e); here ▲: ECG R-peak, ▼: PPG peak; the RR, SPSP and discarded SPSP intervals are reported in blue, red and black, respectively

2) If a single PPG peak is detected between a pair of R-peaks, then it is regarded as a True Positive (TP).
3) If multiple PPG peaks are identified between a pair of R-peaks, then the first peak is regarded as a TP and all other peaks are regarded as False Positives (FP).

Choosing a performance metric is non-trivial in this problem. Hence, we follow the prior arts [25], [18] and choose Detection Error Rate (DER), Precision (PR) and Recall (RC), which are defined below.

$$DER = (FP+FN)/TS \tag{2}$$

$$PR = TP/(TP+FP) \tag{3}$$

$$RC = TP/(TP+FN) \tag{4}$$

where, TS is the total number of R-peaks present in ECG.

The mean (DER_m, PR_m, RC_m) and standard deviation (DER_s, PR_s, RC_s) of the metrics over all subjects are reported in this paper. For a correctly identified (TP) peak, the SPSP interval following the peak is compared with the immediately preceding ground truth RR interval and the mean and standard deviation of the absolute error between the two, denoted by AE_m and AE_s respectively, are evaluated. Further the average number of instructions (INS_m) required to process each subject's data is obtained using the *perfstat* command in Linux [26] and the same is reported as a measure of the computational complexity of the proposed method. In order to avoid the burden of comparing multiple performance metrics for selecting the best method, a *Composite Metric* (CM) is proposed as follows.

$$CM = \prod_i \frac{m_i}{max(\mathbf{M_i})} \tag{5}$$

where, $\mathbf{M_1} = DER_m, \mathbf{M_2} = DER_s, \mathbf{M_3} = AE_m, \mathbf{M_4} = AE_s$ and $\mathbf{M_5} = INS_m$. Evidently lower the value of CM, better is the performance of the algorithm. Here metrics PR and RC are not considered in the definition of CM given in (5), as minimization of DER ensures their maximization.

B. Performance Comparison

Table I suggests that CM gradually improves from Baseline 1 to Final Method. In Baseline 2, better result is obtained when RLS and SSA are used in unison than any one of the two in individual. Moreover different peak correction methods of Baseline 3 are found to produce marginal improvements over Baseline 2. Among these, weighted local interpolation yields the best metric values while incurring the least computational complexity. Though introduction of the outlier removal block in the Final Method increases DER_m and DER_s by 1.03 and 1.07 times respectively, it reduces AE_m and AE_s by 1.04 and 1.08 times respectively. This effect is attributed to the identification and subsequent rejection of the incorrigible parts of the PPG signal. The reductions in AE_m and AE_s outweigh the increases in DER_m and DER_s and CM is found to be the least (92×10^{-5}) in case of this method. Thus the last row of Table I presents the proposed best method for PPG-based beat-to-beat interval extraction. The rest of the analysis is done by considering this methodology only.

C. Segment-wise Performance Analysis

The performance metrics during different motion segments are shown in Table II. The significantly high values of PR and RC for all segments confirm that the algorithm is unbiased. It can be observed that the obtained AE_m and AE_s values are the best during fast run, followed by rest and slow run respectively. High speed running involves rhythmic movements of the body. Hence it introduces rhythmic interference in the PPG which is easy to remove by motion artefact removal

TABLE I
PERFORMANCE ANALYSIS OF DIFFERENT STAGES OF THE PROPOSED ALGORITHM

Method		$DER_m(DER_s)$ (%)	$PR_m(PR_s)$ (%)	$RC_m(RC_s)$ (%)	$AE_m(AE_s)$ (ms)	INS_m $(\times 10^{10})$	CM $(\times 10^{-5})$
Baseline 1		14.68 (5.82)	89.13 (4.20)	97.46 (3.79)	70.50 (96.91)	2.26	45k
Baseline 2	Only RLS	11.25 (4.62)	91.26 (2.98)	98.26 (2.90)	57.30 (98.87)	2.98	30k
	Only SSA	7.90 (7.86)	94.76 (4.99)	97.84 (6.39)	37.34 (70.32)	2.71	15k
	RLS + SSA	1.72 (1.48)	98.91 (0.90)	99.38 (0.65)	11.89 (31.59)	3.41	112
Baseline 3	Weighted Local Interpolation	1.63 (1.33)	98.96 (0.84)	99.43 (0.57)	11.80 (31.10)	3.42	94
	Polynomial Fitting	1.66 (1.25)	98.91 (0.79)	99.43 (0.54)	11.89 (31.50)	3.61	97
	Global Interpolation	1.71 (1.20)	98.83 (0.77)	99.47 (0.52)	12.43 (35.66)	3.49	110
Final method		**1.68 (1.42)**	**99.05 (0.86)**	**99.27 (0.60)**	**11.32 (28.78)**	**3.45**	**92**

TABLE II

SEGMENT-WISE PERFORMANCE ANALYSIS

Segment	DER_m (DER_s)(%)	PR_m (PR_s)(%)	RC_m (RC_s)(%)	AE_m (AE_s)(ms)
Rest	0.98 (1.13)	99.54 (0.65)	99.49 (0.88)	12.37 (23.58)
6-8 Km/Hr Run	2.10 (1.99)	98.62 (1.33)	99.31 (0.72)	13.84 (35.18)
12-15 Km/Hr Run	1.25 (1.73)	99.39 (0.92)	99.36 (0.82)	7.85 (15.63)

procedures. Thus the superior performance metrics for this segment are justified. Though the rest segment should ideally produce the best performance, lower values of AE_m and AE_s are attained for this segment. This is because of the fact that the rest dataset contains brief hand movements which are random, thereby diminishing the performance of the motion artefact removal module. Lastly, the relatively inferior performance of the proposed algorithm for 6-8 km/hr run segment is attributed to the randomness of body movements during the slow running event.

Fig. 8 shows the scatter plots and Bland-Altman (BA) plots between the ECG RR intervals and the PPG SPSP intervals during different motion segments. Though most of the mentioned plot parameters suggest that the proposed algorithm can track SPSP intervals from noisy PPG, the significantly high ranges of Line of agreement (LOA) of BA plots indicate that the precision requires further enhancement.

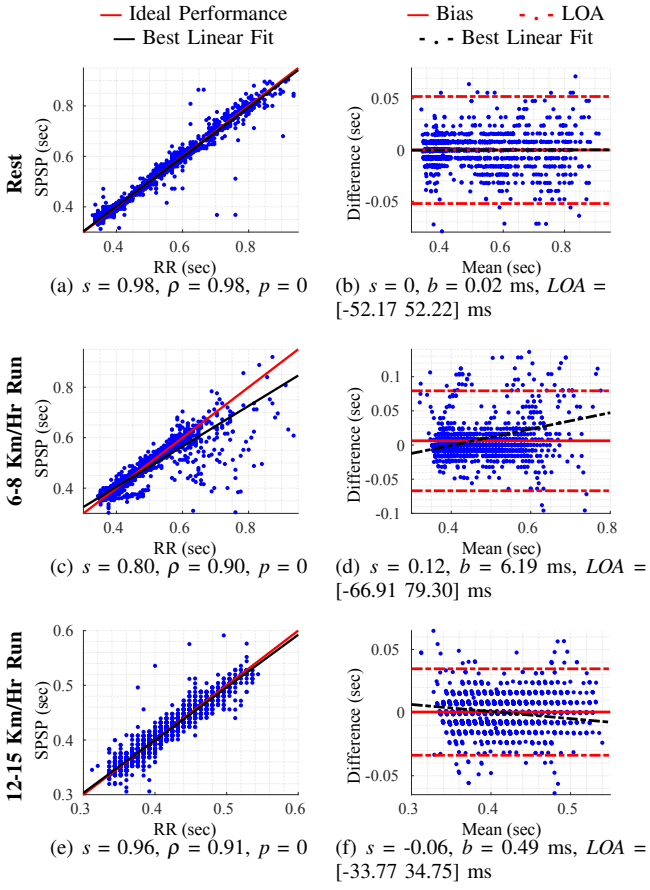

(a) s = 0.98, ρ = 0.98, p = 0 (b) s = 0, b = 0.02 ms, LOA = [-52.17 52.22] ms

(c) s = 0.80, ρ = 0.90, p = 0 (d) s = 0.12, b = 6.19 ms, LOA = [-66.91 79.30] ms

(e) s = 0.96, ρ = 0.91, p = 0 (f) s = -0.06, b = 0.49 ms, LOA = [-33.77 34.75] ms

Fig. 8. Scatter [(a), (c), (e)] and BA [(b), (d), (f)] plots between RR and SPSP intervals for different motion segments; here, s = Slope of linear fit, ρ = Pearson correlation, p = P-value, b = bias and LOA = Line of agreement

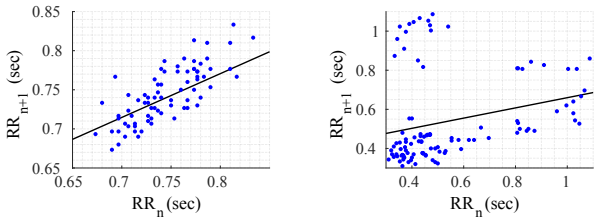

Fig. 9. Representative Poincare plots - healthy (left) and AF (right) subjects

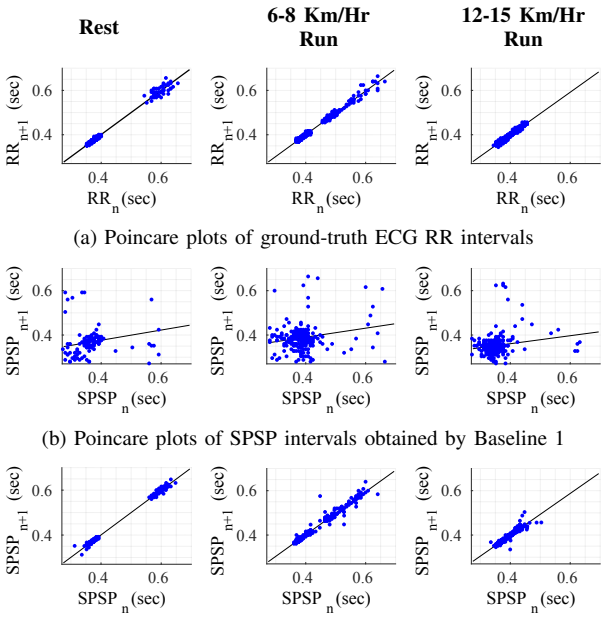

(a) Poincare plots of ground-truth ECG RR intervals

(b) Poincare plots of SPSP intervals obtained by Baseline 1

(c) Poincare plots of SPSP intervals obtained by Final Method

Fig. 10. Poincare Analysis on Subject 12: black line shows best linear fit

D. Poincare Analysis

The Poincare Plot of beat-to-beat intervals is proven to have visually distinct structure for healthy individuals and AF patients (Fig. 9). It looks like a *comet* for a healthy subject and is *wedge-shaped* for an AF patient [27]. Fig. 10(a) shows the ground truth RR interval Poincare Plots for different motion segments, for subject 12. The shapes of the plots confirm that the subject is healthy. Though two distinct clusters can be seen in the plot for rest, it is expected. During the initial rest period of the experiment, the subject's heart rate remains low and the RR intervals remain high. However during the last rest segment after extensive running, the heart rate increases, thereby decreasing the RR intervals. Same argument holds for the 6-8 km/hr run segment. Now, Fig. 10(b) shows the plots obtained from PPG SPSP intervals detected by preprocessing and peak detection only (Baseline 1) for the same subject. Seeing these plots the subject can be wrongly identified as an AF patient. When using the final pipeline of the proposed algorithm, the plots become as given in Fig. 10(c). Evidently the shapes of these plots match those of the ground truth given in Fig. 10(a). Thus, though the motion artefacts can make a healthy subject look like an AF patient as shown in Fig. 10(b), the proposed algorithm can effectively eliminate the artefacts to restore proper features. However, the proposed method is yet to be validated on AF patients due to the unavailability of such patients' PPG-ECG

TABLE III
COMPARISON WITH PRIOR ART

Method (Signals used)	DER_m (DER_s) (%)	PR_m (PR_s) (%)	RC_m (RC_s) (%)	AE_m (AE_s) (ms)	INS_m ($\times 10^{10}$)
[16] (PPG & Acc)	27.46 (6.28)	85.84 (3.26)	86.53 (3.57)	64.97 (86.28)	2.41
[17] (PPG)	21.14 (3.99)	83.84 (3.26)	97.97 (3.13)	94.36 (111.86)	2.16
[18] (PPG)	38.16 (3.92)	78.94 (4.01)	84.85 (3.41)	163.59 (140.57)	29.82
Proposed (PPG & Acc)	**1.68 (1.42)**	**99.05 (0.86)**	**99.27 (0.60)**	**11.32 (28.78)**	**3.45**

data during movements.

E. Comparison with Prior Art

Majority of the existing works on noisy PPG had the goal of average heart-rate estimation over a certain time period (e.g. 8 sec window with 6 sec overlap) [9]–[14], for which primarily frequency domain analysis were performed. Those works did not attempt to identify the beat-to-beat cardiac cycles which is the main objective for our application. So those cannot be compared with the current method. Rather, the time-domain approaches [16]–[18] are chosen for comparison. Among these, the work [16] is particularly relevant as it performed adaptive LMS filtering using acceleration signals. Though INS_m for the proposed method is 1.4 and 1.6 times higher than those of [16] and [17] respectively, the other metrics listed in Table III confirm that the proposed approach significantly outperforms the existing techniques.

V. CONCLUSIONS

This paper proposes an automated 24x7 beat-to-beat interval estimation algorithm using wearable PPG. This method can handle the artefacts arising from daily life motion by RLS and SSA. The portions of PPG which can not be reconstructed by the proposed method are automatically marked as incorrigible. The proposed algorithm is found to perform well on extensive cases of movements like running, achieving 1.68% DER_m and 11.32 ms AE_m. However the performance during slower run is poorer than that during fast run. It is attributed to the inherent randomness of body movements during slow run. This round-the-clock cardiac cycle monitoring solution can be a potential choice for non-invasive screening of AF and other arrhythmia. However validation of the proposed pipeline on AF subjects' data remains as a future work.

REFERENCES

[1] J. Albarran, "A race against time: the challenge of cardiovascular disease in developing economies," *Nursing in Critical Care*, vol. 9, no. 5, p. 250, 2004.

[2] D. Prabhakaran, P. Jeemon, and A. Roy, "Cardiovascular diseases in India: current epidemiology and future directions," *Circulation*, vol. 133, no. 16, pp. 1605–1620, 2016.

[3] W. H. O. *et al.*, "International statistical classification of diseases and related health problems: 10^{th} revision (ICD-10)," https://icd.who.int/browse10/2016/en, 1992, [Online; accessed 14-February-2019].

[4] R. Banerjee, R. Vempada, K. Mandana, A. D. Choudhury, and A. Pal, "Identifying coronary artery disease from photoplethysmogram," in *Proceedings of the International Joint Conference on Pervasive and Ubiquitous Computing: Adjunct*. ACM, 2016, pp. 1084–1088.

[5] R. Banerjee, A. D. Choudhury, S. Datta, A. Pal, and K. M. Mandana, "Non-invasive detection of coronary artery disease using PCG and PPG," in *eHealth 360°*. Springer, 2017, pp. 241–252.

[6] G. D. Clifford, C. Liu, B. Moody, L.-w. H. Lehman, I. Silva, Q. Li, A. Johnson, and R. G. Mark, "AF classification from a short single lead ECG recording: The Physionet Computing in Cardiology Challenge 2017," *Proceedings of Computing in Cardiology*, vol. 44, p. 1, 2017.

[7] A. Mukherjee, A. D. Choudhury, S. Datta, C. Puri, R. Banerjee, R. Singh, A. Ukil, S. Bandyopadhyay, A. Pal, and S. Khandelwal, "Detection of atrial fibrillation and other abnormal rhythms from ECG using a multi-layer classifier architecture," *Physiological Measurement*, 2019.

[8] https://www.empatica.com/, [Online; accessed 14-Feb-2019].

[9] Z. Zhang, Z. Pi, and B. Liu, "TROIKA: A general framework for heart rate monitoring using wrist-type photoplethysmographic signals during intensive physical exercise," *IEEE Transactions on biomedical engineering*, vol. 62, no. 2, pp. 522–531, 2015.

[10] Z. Zhang *et al.*, "Photoplethysmography-based heart rate monitoring in physical activities via joint sparse spectrum reconstruction." *IEEE Trans. Biomed. Engineering*, vol. 62, no. 8, pp. 1902–1910, 2015.

[11] Y. Ye, Y. Cheng, W. He, M. Hou, and Z. Zhang, "Combining nonlinear adaptive filtering and signal decomposition for motion artifact removal in wearable photoplethysmography," *IEEE Sensors Journal*, vol. 16, no. 19, pp. 7133–7141, 2016.

[12] M. B. Mashhadi, M. Essalat, M. Ahmadi, and F. Marvasti, "An improved algorithm for heart rate tracking during physical exercise using simultaneous wrist-type photoplethysmographic (PPG) and acceleration signals," in *Biomedical Engineering and 1st International Iranian Conference on (ICBME), 23rd Iranian Conference on*. IEEE, 2016, pp. 146–149.

[13] Q. Xie, Q. Zhang, G. Wang, and Y. Lian, "Combining adaptive filter and phase vocoder for heart rate monitoring using photoplethysmography during physical exercise," in *40th Annual International Conference of the IEEE Engineering in Medicine and Biology Society (EMBC)*, 2018, pp. 3568–3571.

[14] J. Xiong, L. Cai, D. Jiang, H. Song, and X. He, "Spectral matrix decomposition-based motion artifacts removal in multi-channel PPG sensor signals." *IEEE Access*, vol. 4, pp. 3076–3086, 2016.

[15] X. Sun, P. Yang, Y. Li, Z. Gao, and Y.-T. Zhang, "Robust heart beat detection from photoplethysmography interlaced with motion artifacts based on empirical mode decomposition," in *Proceedings of 2012 IEEE-EMBS International Conference on Biomedical and Health Informatics*, 2012, pp. 775–778.

[16] H. Han and J. Kim, "Artifacts in wearable photoplethysmographs during daily life motions and their reduction with least mean square based active noise cancellation method," *Computers in biology and medicine*, vol. 42, no. 4, pp. 387–393, 2012.

[17] D.-G. Jang, S. Park, M. Hahn, and S.-H. Park, "A real-time pulse peak detection algorithm for the photoplethysmogram," *Int. J. Electron. Electr. Engin*, vol. 2, pp. 45–49, 2014.

[18] S. Vadrevu and M. S. Manikandan, "A robust pulse onset and peak detection method for automated PPG signal analysis system," *IEEE Transactions on Instrumentation and Measurement*, no. 99, pp. 1–11, 2018.

[19] https://www.mayoclinic.org/healthy-lifestyle/fitness/expert-answers/heart-rate/faq-20057979, [Online; accessed 11-Feb-2019].

[20] https://www.heart.org/en/healthy-living/fitness/fitness-basics/target-heart-rates, [Online; accessed 11-Feb-2019].

[21] J. G. Proakis and D. G. Manolakis, *Digital signal processing: principles, algorithms, and applications*. Pearson Prentice Hall, 2007.

[22] S. Sanei and H. Hassani, *Singular spectrum analysis of biomedical signals*. CRC Press, 2015.

[23] S. W. Keet, C. S. Bulte, R. P. Garnier, C. Boer, and R. A. Bouwman, "Short-term heart rate variability in healthy adults," *Anaesthesia*, vol. 68, no. 7, pp. 775–777, 2013.

[24] A. E. Johnson, J. Behar, F. Andreotti, G. D. Clifford, and J. Oster, "Multimodal heart beat detection using signal quality indices," *Physiological measurement*, vol. 36, no. 8, p. 1665, 2015.

[25] J. Pan and W. J. Tompkins, "A real-time QRS detection algorithm," *IEEE Trans. Biomed. Eng*, vol. 32, no. 3, pp. 230–236, 1985.

[26] https://linux.die.net/man/1/perf-stat, [Online; accessed 19-Feb-2019].

[27] T. S. Henriques, S. Mariani, A. Burykin, F. Rodrigues, T. F. Silva, and A. L. Goldberger, "Multiscale Poincaré plots for visualizing the structure of heartbeat time series," *BMC medical informatics and decision making*, vol. 16, no. 1, p. 17, 2015.